

# Coordinate-based co-localization-mediated analysis of arrestin clustering upon stimulation of the C–C chemokine receptor 5 with RANTES/CCL5 analogues

Laura Tarancón Díez · Claudia Bönsch · Sebastian Malkusch · Zinnia Truan · Mihaela Munteanu · Mike Heilemann · Oliver Hartley · Ulrike Endesfelder · Alexandre Fürstenberg

Accepted: 25 February 2014 / Published online: 13 March 2014  
© Springer-Verlag Berlin Heidelberg 2014

**Abstract** G protein-coupled receptor activation and desensitization leads to recruitment of arrestin proteins from cytosolic pools to the cell membrane where they form clusters difficult to characterize due to their small size and further mediate receptor internalization. We quantitatively investigated clustering of arrestin 3 induced by potent anti-HIV analogues of the chemokine RANTES after stimulation of the C–C chemokine receptor 5 using single-molecule localization-based super-resolution microscopy. We determined arrestin 3 cluster sizes and relative fractions of arrestin 3 molecules in each cluster through image-based analysis of the localization data by adapting a method originally developed for co-localization analysis from molecular coordinates. We found that only classical agonists in the set of tested ligands were able to efficiently recruit arrestin 3 to clusters mostly larger than 150 nm in size and compare our results with existing data on arrestin 2 clustering induced by the same chemokine analogues.

**Electronic supplementary material** The online version of this article (doi:10.1007/s00418-014-1206-1) contains supplementary material, which is available to authorized users.

L. Tarancón Díez · Z. Truan · A. Fürstenberg (✉)  
Department of Human Protein Sciences, University of Geneva,  
CMU, Rue Michel-Servet 1, 1211 Geneva 4, Switzerland  
e-mail: alexandre.fuerstenberg@unige.ch

C. Bönsch · M. Munteanu · O. Hartley  
Department of Pathology and Immunology,  
University of Geneva, CMU, Rue Michel-Servet 1,  
1211 Geneva 4, Switzerland

S. Malkusch · M. Heilemann · U. Endesfelder  
Institute for Physical and Theoretical Chemistry,  
Goethe-University Frankfurt, Max-von-Laue-Str. 7,  
60438 Frankfurt, Germany

**Keywords** Clustering · Super-resolution microscopy · Single-molecule localization microscopy · G protein-coupled receptors · Arrestin · CCR5

## Introduction

G protein-coupled receptors (GPCRs) are membrane proteins that mediate a wide range of chemical signals across the cell membrane and thereby control important physiological processes. Not surprisingly, they have therefore been major drug targets (Rask-Andersen et al. 2011). Activation of a GPCR through agonist binding (ions, small molecules, hormones,...) induces dissociation of its cytosolic G protein, leading to downstream second messenger signalling (Rosenbaum et al. 2009). In parallel, arrestin proteins are recruited from cytosolic pools (Lefkowitz and Shenoy 2005). They arrest coupling between G proteins and their receptor and, independently of G protein signalling, also induce clathrin-mediated endocytosis as part of a desensitization process common to GPCRs (Moore et al. 2007). Not all agonists trigger, however, the full signalling repertoire of GPCRs and there are now numerous examples of ligands that bias the receptor response either towards G protein coupling or towards non-G protein effectors such as arrestins (Gesty-Palmer and Luttrell 2011). This ability of different ligands binding to the same GPCR to trigger various pharmacological outcomes is related to the diversity of conformational states in which GPCRs exist (Kobilka and Deupi 2007; Bockenhauer et al. 2011) and has become an attractive feature for drug discovery (Kenakin and Christopoulos 2013).

The C–C chemokine receptor 5 (CCR5) is a prototypical GPCR for which the existence of biased ligands has been suggested (Zidar 2011; Kenakin et al. 2012).

**Table 1** Functional characterization of RANTES (Hartley et al. 2004; Gaertner et al. 2008b) and of some of its analogues (Gaertner et al. 2008a)

Ligand	Anti-HIV potency	G protein signalling (%)	CCR5 internalization (%)
RANTES	~1 $\mu$ M	50	64
PSC-RANTES	25 pM	100	100
6P4-RANTES	21 pM	88	93
5P12-RANTES	28 pM	<5	3
5P14-RANTES	26 pM	<5	47

G protein signalling activity (release of  $\text{Ca}^{2+}$ ) and CCR5 internalization are expressed relatively to PSC-RANTES, which displays maximal response in these assays

It is further an important drug target by being the major co-receptor used by HIV to infect target cells, and it can be efficiently blocked to prevent person-to-person virus transmission (Kuhmann and Hartley 2008; Karim et al. 2010). Analogues of the natural CCR5 ligand RANTES were previously shown to efficiently prevent HIV infection (Lederman et al. 2004; Hartley et al. 2004; Gaertner et al. 2008a). Interestingly, however, the pharmacological profiles of these ligands differing by only a few amino acids among the first 9 of 68 residues (Table S1) display large variations (Table 1). Molecules such as RANTES, 6P4-RANTES, or PSC-RANTES act like classical partial or full agonists by causing both strong G protein activation and CCR5 internalization. The increased anti-HIV potency of PSC-RANTES over RANTES has been ascribed to additional long-term sequestration of CCR5 inside target cells (Escola et al. 2010). On the other hand, analogues such as 5P12-RANTES and 5P14-RANTES display the same anti-HIV activity as PSC-RANTES or 6P4-RANTES but do not trigger G protein signalling and induce CCR5 internalization only partially (5P14-RANTES) or not at all (5P12-RANTES). It is currently not understood how these chemokine analogues all potently block HIV infection despite their very different pharmacological profiles, but stabilization of CCR5 into various conformational ensembles is likely involved. We recently characterized the effect of some of these ligands on arrestin 2 recruitment upon stimulation of CCR5 to test whether arrestin 2 mobilization could relate to their pharmacology and found that only those ligands capable of recruiting arrestin 2 also induced receptor internalization (Truan et al. 2013).

Among the arrestin protein family, both arrestin 2 and arrestin 3 are ubiquitously expressed. These proteins interact with most GPCRs and cluster around clathrin-coated pits upon GPCR stimulation (Santini et al. 2002; Laporte et al. 2000; Luttrell et al. 1999). It has, however, traditionally been difficult to study the formation, the dimension, or the fate of such clusters by standard imaging procedures because of their size near or below the diffraction limit. Standard techniques applied to obtain information on

biomolecular interactions such as Förster resonance energy transfer (FRET) or two-colour co-localization of differently labelled molecules by fluorescence microscopy indeed suffer from a spatial resolution limited to typically ~200 nm because of the wave-like nature of visible light. The recent introduction of super-resolution microscopy techniques has enabled to overcome this limit (Rust et al. 2006; Betzig et al. 2006; Hess et al. 2006; Hell 2007) and opened up new avenues to resolve small objects and monitor protein–protein interaction scales closer to the molecular resolution. Super-resolution methods based on the localization of single molecules (Fürstenberg and Heilemann 2013; Moerner 2012) have the advantage of providing not only an image (which means pixels with an intensity information) but also molecular coordinates that can be directly used in novel schemes for co-localization and clustering analysis (Sengupta et al. 2011; Malkusch et al. 2012; Owen et al. 2013; Truan et al. 2013; Endesfelder et al. 2013; Specht et al. 2013).

Clustering and oligomerization are frequent types of functionally relevant protein–protein interaction in which two or several proteins of the same kind interact together. From an analysis point of view, they are, however, only a particular case of molecular entities interacting together, so that existing co-localization analysis methods based on molecular coordinates can readily be adapted to monitor clustering processes. We present here a simple modification to a recently introduced coordinate-based co-localization (CBC) analysis method (Malkusch et al. 2012) that enables to evaluate the spatial distribution of a protein recorded in a single channel and provides a physical basis for setting a threshold in image-based cluster analysis. We apply CBC-mediated cluster analysis to evaluate the dimension of arrestin 3 clusters upon stimulation of CCR5 by RANTES analogues in order to test the hypothesis that these ligands induce differential arrestin 3 recruitment and relate this observation to their pharmacological profile. We further compare our results with recently obtained information on arrestin 2 mobilization by a similar set of ligands (Truan et al. 2013) and find that most ligands causing arrestin 2

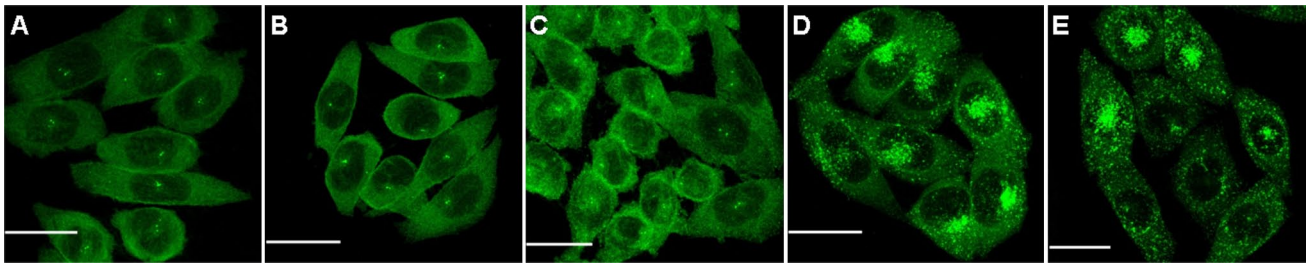


**Fig. 1** Confocal microscopy images (maximum intensity projection) of arrestin 3-GFP in fixed CHO-CCR5 cells in the absence of ligand (a) or after 90 min of stimulation with 5P12-RANTES (b), 5P14-RANTES (c), RANTES (d), or PSC-RANTES (e). Scale bar 20  $\mu\text{m}$

clustering also cause arrestin 3 clustering, except 5P14-RANTES. This compound might thereby represent the first example of a ligand inducing recruitment of selectively one type of arrestin upon stimulation of CCR5.

## Materials and methods

### Materials, cell lines, and cell culture

All cell culture reagents were obtained from Life Technologies. Water was purified using a Milli-Q system (Millipore). RANTES and its analogues were prepared by total chemical synthesis as previously published (Gaertner et al. 2008a).

Plasmids pEGFP-N1 with bovine arrestin 3 (Mundell et al. 2000) were a gift from Jeffrey Benovic (Thomas Jefferson University). Chinese hamster ovary cells stably expressing CCR5 (hereafter CHO-CCR5) (Hartley et al. 2004) were transfected with 0.5  $\mu\text{g}$  arrestin 3-GFP plasmid, and stable clones were obtained as described before (Truan et al. 2013).

Cells were cultured at 37  $^{\circ}\text{C}$  with 5 %  $\text{CO}_2$  in phenol-red free RPMI supplemented with 10 % foetal bovine serum, 100 units/ml penicillin, and 100  $\mu\text{g}/\text{ml}$  streptomycin. For super-resolution experiments, they were plated 36–72 h beforehand on glass-bottom petri dishes (FluoroDish<sup>TM</sup>, World Precision Instruments, Inc.) coated with fibronectin (Calbiochem).

### Immunofluorescence

Samples for confocal microscopy and for super-resolution imaging were prepared by fixation in 4 % paraformaldehyde as previously described (Truan et al. 2013). For super-resolution imaging, samples were further stained with a GFP-specific ATTO655-labelled GFP-Trap<sup>®</sup> nanobody (ChromoTek) (Truan et al. 2013). When desired, samples were treated with 100 nM chemokine analogues in full medium 90 min before fixation.

### Confocal microscopy

Stacks of confocal microscopy images were recorded on a Zeiss LSM700 microscope with an X63/1.4NA Plan Apochromat oil-immersion objective. Excitation was performed with the 488 nm line of an Ar/Kr laser, and GFP filters were used for detection. Maximum intensity projections as displayed in Fig. 1 were obtained using the ZEN 2011 software.

### Super-resolution microscopy

Super-resolution experiments were performed on a wide-field epi-fluorescence microscope (Truan et al. 2013) with the *d*STORM (direct stochastic optical reconstruction microscopy) technique (Heilemann et al. 2009) using 640 nm excitation ( $\sim 3 \text{ kW}/\text{cm}^2$ , Coherent Cube 640-100-C laser). Blinking of ATTO655 was induced with a 50  $\mu\text{M}$  solution of ascorbic acid (Merck) (Cordes et al. 2010) in heavy water ( $\text{D}_2\text{O}$ , 99.8 % D-atom content, Armar Chemicals) (Lee et al. 2013) prepared from a 1-mM stock solution in  $\text{H}_2\text{O}$ . Single emitters were localized, and super-resolution images ( $10 \times 10 \text{ nm}^2$  per pixel) were reconstructed with the *rapid*STORM software (version 2.13) (Wolter et al. 2010). Each pixel on the EMCCD camera (Andor iXonEM+ DU8987) corresponded to a  $109 \times 109 \text{ nm}^2$  area in the sample plane.

### Cluster analysis

Ripley's H-function (normalized form of the K-function) (Ripley 1977) was calculated as previously described (Truan et al. 2013) for  $5 \times 5 \mu\text{m}^2$  regions of interest using a self-written MATLAB (The MathWorks, Inc.) routine, and edge effects were taken into account by omitting molecules closer than 1  $\mu\text{m}$  from the edge of the region of interest in the calculations.

Coordinate-based co-localization (CBC)-mediated cluster analysis was performed using an algorithm described elsewhere (Malkusch et al. 2012). Because the algorithm

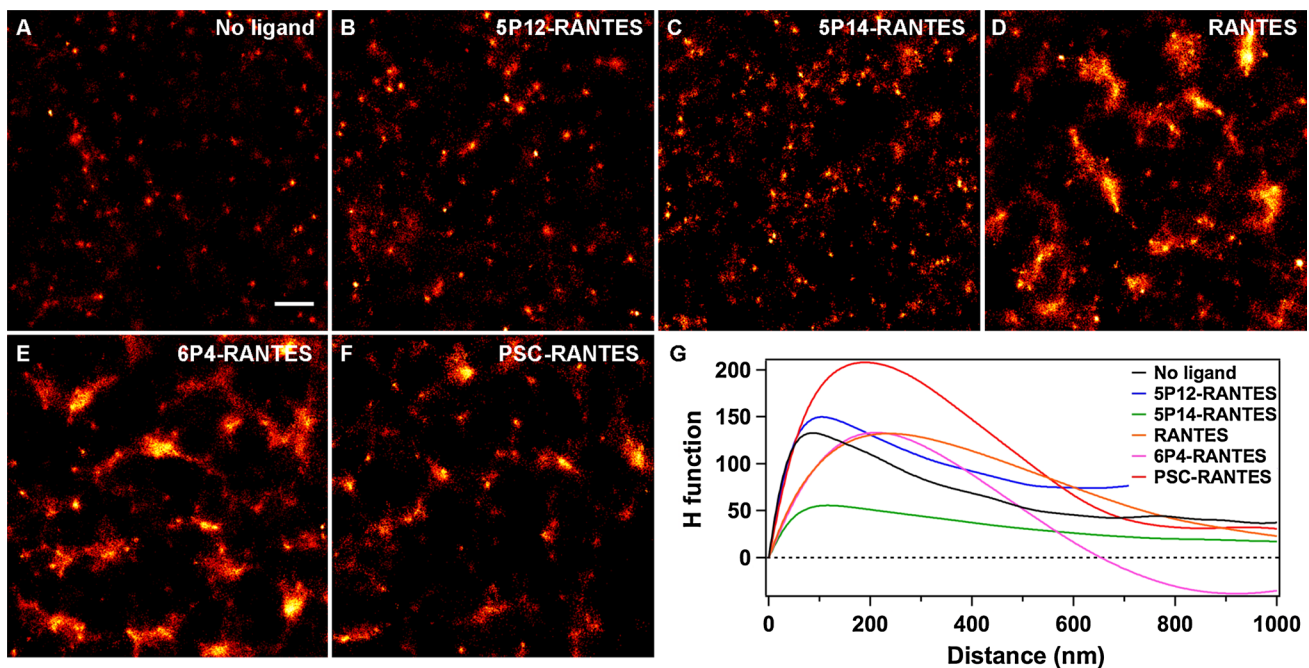


**Fig. 2** Representative super-resolution images of ATTO655-nanobody-labelled arrestin 3-GFP in fixed CHO-CCR5 in the absence of ligand (**a**) and after treatment with different chemokine analogues for 90 min (**b–f**). Scale bar 0.5  $\mu\text{m}$ . **g** Ripley analysis of the *d*STORM

experiments demonstrating clustering of arrestin 3 upon stimulation of CCR5 with RANTES, 6P4-RANTES, and PSC-RANTES, but not with 5P12-RANTES or 5P14-RANTES. The peak position is indicative of the typical cluster size

was originally written to determine co-localization of two molecules, it requires data from two channels as an input. Our data was, however, recorded in a single channel since our goal was to measure clustering of a single species. We therefore performed pre-sorting of the detected arrestin 3 molecules into molecules that were localized in odd frames and molecules that were localized in even frames, resulting in two localization files that both contain information about the distribution of the same molecules within the range of the localization accuracy (Banterle et al. 2013; Nieuwenhuizen et al. 2013). By correlating the circular distributions of the arrestin 3 molecule, localizations from both localization lists around a single arrestin 3 molecule with each other (Malkusch et al. 2012), a clustering value characterizing the degree of clustering could be determined for every localization. This parameter can vary between  $-1$  and  $1$ , a value of  $1$  indicating the highest probability of clustering.

Localizations with clustering values above  $0.7$  were kept for morphological cluster analysis (custom-written software), which was performed by applying a  $15\text{-nm}$  Gaussian filter and a binary mask to the filtered data. Cluster sizes were extracted from cohesive regions in the mask, and the area of every cluster was further weighted by the integrated fluorescence intensities within every cluster to determine the fraction of arrestin 3 molecules per cluster. Cluster radii were calculated from spheres coextensive to the measured clusters.

## Results

In order to visualize arrestin 3, we stably transfected CHO cells expressing CCR5 with a plasmid for arrestin 3 carrying a GFP fusion tag (Mundell et al. 2000). Like arrestin 2, arrestin 3 proteins are randomly distributed in the cytoplasm of resting cells (Fig. 1a). The distribution did not change when cells were exposed to a saturating concentration of 5P12-RANTES or of 5P14-RANTES (Fig. 1b, c). However, upon CCR5 stimulation with the agonists RANTES and PSC-RANTES (Fig. 1d, e), arrestin 3 molecules were recruited from the cytosolic pool to the plasma membrane where they formed clusters (Laporte et al. 2000) with dimensions around the diffraction limit, making it difficult to investigate their morphology in a robust way by classical microscopy techniques.

We, thus, turned to super-resolution microscopy so as to quantify the magnitude of arrestin 3 recruitment by determining the size of these clusters and the relative number of arrestin 3 molecules within each cluster, using an approach that we recently successfully applied to the investigation of arrestin 2 clustering and that relies on dye-labelled nanobodies selective for GFP (Truan et al. 2013; Ries et al. 2012). Super-resolution images of arrestin 3 were obtained in untreated cells and in cells exposed to the different chemokine analogues (Fig. 2a–f, Fig. S1). Images of cells treated with no ligand, with 5P12-RANTES, or

with 5P14-RANTES display mainly individual proteins and small clusters, whereas much larger clusters are frequently visualized in cells stimulated with RANTES, 6P4-RANTES, or PSC-RANTES. In order to quantify clustering, we calculated Ripley's H-function from the single-molecule coordinates obtained in the super-resolution experiment (Fig. 2g). This function is a straightforward way of characterizing the randomness of a spatial distribution. Positive values indicate that molecules are closer to each other than if they were homogeneously distributed, which denotes clustering, and the value at which the function peaks is indicative of the average cluster size (its value is comprised between the average cluster radius and diameter). Displacement of the peak to larger values with RANTES, 6P4-RANTES, and PSC-RANTES compared with untreated cells, but not with 5P12-RANTES or 5P14-RANTES, confirmed that the former 3 ligands selectively induce strong arrestin 3 clustering.

We next aimed at quantifying the dimensions of arrestin 3 clusters by image-based analysis of the super-resolution data (Malkusch et al. 2013; Endesfelder et al. 2013; Truan et al. 2013). The goal of such analysis is to generate from each super-resolution image a binary cluster map in which every cohesive region represents a cluster whose size can then be determined by integration. Creating a binary map from a super-resolution image, which contains intensity information, requires, however, the application of an intensity threshold to the *d*STORM image to define cluster boundaries. In order to identify which localizations are part of a cluster based on a clustering parameter that can be calculated, we adapted an algorithm originally developed to assess co-localization from single-molecule coordinates (Malkusch et al. 2012), considering that clustering is only a special case of co-localization in which all the information is collected in a single colour channel instead of two. Our coordinate-based co-localization (CBC)-mediated clustering algorithm (Fig. 3a) splits the list of coordinates obtained from a *d*STORM experiment (which is also used to reconstruct super-resolution images such as in Fig. 3b, c) into two, as if the data had been recorded in two channels, and calculates a clustering value for every localization, which takes into account its direct neighbourhood (for details, see "Materials and methods" section). This clustering value can vary from  $-1$  for anti-correlated distributions through  $0$  for uncorrelated distributions up to  $1$  for perfectly correlated distributions, which would indicate a high probability of clustering. It was previously shown for co-localization analysis that overlaying two identical images with a translational shift of  $10$  nm results in the largest fraction of the distribution of co-localization values (analogous to the clustering values here) being above  $0.7$  (Malkusch et al. 2012). Given the typical localization precision in our super-resolution experiments of about  $20$  nm,

we used a minimal clustering value of  $0.7$  as a threshold to consider a localization as being part of a cluster and filtered out localizations with a clustering value below this threshold. CBC-mediated clustering images (Fig. 3d, e, Fig. S2) in which localizations with a clustering value above threshold are displayed in green and those below threshold in red show that rejected localizations mostly either form a cloud-like pattern throughout the cell indicative of single or spurious localizations or can be found at the edges of higher intensity clustered areas, thereby defining the border of clusters.

After application of the CBC-mediated clustering filter to all images, cluster maps were extracted (Fig. 3f, g, Fig. S3) by applying a  $15$ -nm Gaussian blur filter, reflecting the finite experimental localization precision (for this reason, the clusters in the binary map, Fig. 3g, appear slightly larger than in the filtered image, Fig. 3e) (Smith et al. 2010). The area of each cohesive region was then calculated and weighted by its integrated fluorescence intensity to gain information on relative arrestin 3 molecule numbers per cluster. Figure 4 shows for each chemokine analogue the fraction of arrestin 3 as a function of cluster size. Cluster radii were calculated from spheres coextensive to the measured cluster area. In untreated cells, most arrestin 3 molecules were found in domains with a radius smaller than  $120$  nm, and no significant change was noticed when cells were exposed to either 5P12-RANTES or 5P14-RANTES, in agreement with the confocal microscopy observations (Fig. 1). The fact that clusters, albeit of small size, are observed for these three conditions for which one could expect to find arrestin 3 homogeneously distributed throughout the cytoplasm can be ascribed to an average number of fluorophores per nanobody higher than one ( $1.5$ ), to multiple detection of the same molecules due to fluorophore blinking, and to the experimental scheme requiring fluorophores to be first put into a dark state at the beginning of the experiment, inevitably leading to random but non-uniform photobleaching of dye molecules before the start of the acquisition. Similar observations were previously made with arrestin 2 (Truan et al. 2013). On the other hand, upon treatment of the cells with the agonists RANTES, 6P4-RANTES, or PSC-RANTES, the largest fraction of arrestin 3 molecules was found in clusters with a radius larger than  $150$  nm, confirming that these ligands that are all classical agonists (that is, they cause G protein activation) lead to strong clustering of arrestin 3 via CCR5.

## Discussion

We have quantitatively investigated the recruitment of arrestin 3 to CCR5 using single-molecule localization microscopy and morphological cluster analysis after

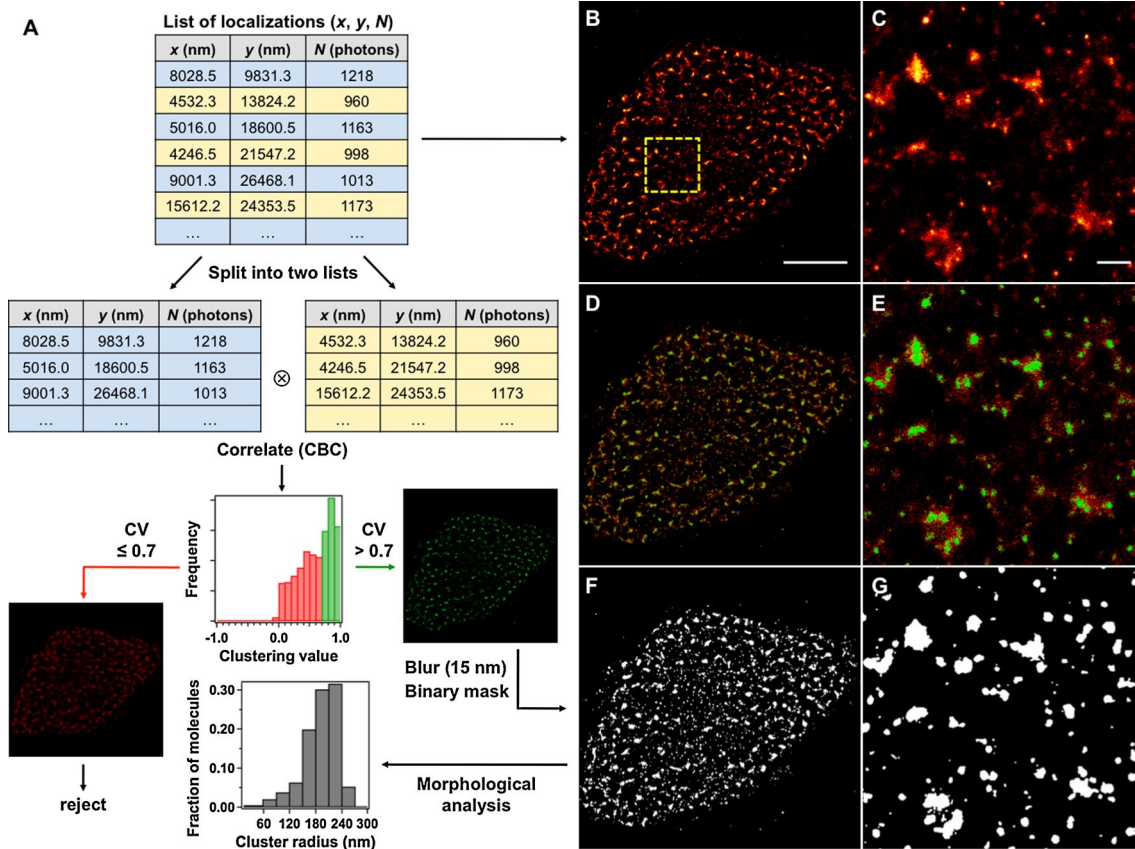
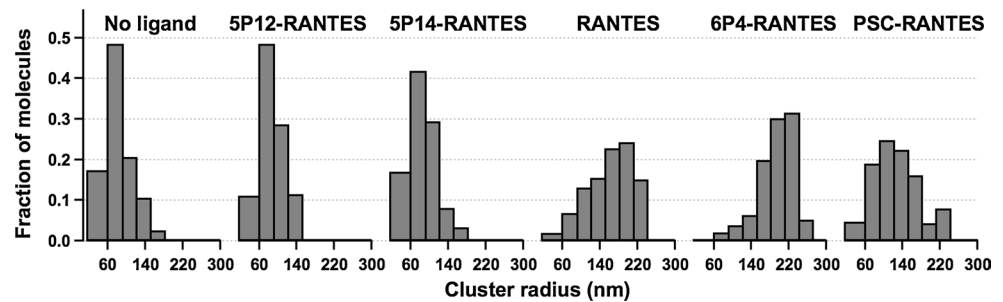


**Fig. 3** **a** Flow chart of CBC-mediated cluster analysis. In CBC-mediated cluster analysis, the table of localizations from the *d*STORM experiment, which is used to reconstruct super-resolution images **b**, **c** is split into two equally long tables of coordinates. A clustering value (CV) is calculated for every localization. Localizations with a clustering value below a 0.7 threshold are discarded. The others are kept to reconstruct a CBC-mediated clustering filtered image which is then blurred with a Gaussian filter to take into account the finite localization precision of the experiment. The resulting binary image (**f**, **g**)

undergoes morphological analysis for cluster sizes and relative molecule numbers from every cluster to be extracted. **b**, **c** Super-resolution images of a cell exposed to 6P4-RANTES. **d**, **e** CBC-mediated clustering filtered images in which every localization with a clustering value below threshold is displayed in *red* and with a clustering value above threshold in *green*. **f**, **g** Binary cluster maps extracted from the blurred CBC-mediated clustering filtered images. The *yellow box* in **b** represents the area blown up in **c**, **e**, and **g**. Scale bar 5  $\mu\text{m}$  in **b**, **d**, **f**; 0.5  $\mu\text{m}$  in **c**, **e**, **g**

**Fig. 4** Distribution of arrestin 3 molecules as a function of cluster size determined from CBC-mediated morphological cluster analysis



stimulation of the receptor with different chemokine analogues. We observed that a saturating concentration of the ligands RANTES, 6P4-RANTES, and PSC-RANTES, which induce both G protein signalling and lead to receptor internalization, induced strong arrestin 3 clustering (Figs. 1, 2), whereas no arrestin 3 recruitment above

background level was observed with 5P12-RANTES and 5P14-RANTES, two ligands that do not activate the G protein and induce no or only partial receptor internalization (Table 1). In order to extract quantitative information from the super-resolution experiments, we introduced a coordinate-based clustering filter derived from a coordinate-based

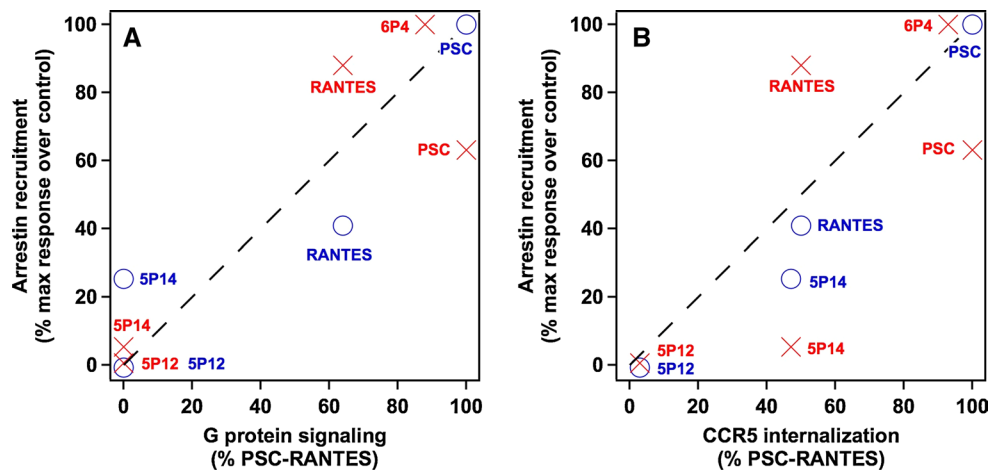


**Fig. 5** Relative arrestin 2 (blue) and arrestin 3 (red) recruitment versus CCR5 internalization (a) or G protein signalling efficiency (b) for the different chemokine analogues. The magnitude of arrestin recruitment was calculated by comparing the fraction of arrestin 3 molecules found in clusters larger than 100 nm (Truan et al. 2013) compared with the control level (0 %), which is defined by observations

in untreated cells. Arrestin 2 data were taken from (Truan et al. 2013) and reanalyzed with the CBC-mediated cluster analysis for proper quantitative comparison (differences for the values obtained by CBC-mediated cluster analysis to the originally published values lie within experimental errors and thus revalidate the visually set threshold values used before)

co-localization analysis method (Malkusch et al. 2012). It enables to sort localizations based on a calculated clustering value that takes into account the spatial distribution around every localization and that can be used as a threshold for image-based cluster analysis (Fig. 3) instead of relying on a visually set manual threshold. We successfully applied this filter to the determination of arrestin 3 cluster sizes and arrestin 3 distribution within these clusters. In agreement with qualitative observations, we found that the largest fraction of arrestin 3 molecules was recruited to domains with a radius of 150 nm or larger with RANTES, 6P4-RANTES, and PSC-RANTES, whereas the distribution stayed unaltered with 5P12-RANTES and 5P14-RANTES compared with cells not exposed to chemokine analogues for which the domains are mostly smaller than 120 nm in radius (Fig. 4).

The finding that, within the tested set of ligands, only classical agonists induce arrestin 3 clustering might suggest a link between arrestin 3 recruitment and G protein activation. The magnitude of arrestin 3 recruitment, calculated as the fraction of molecules found in clusters larger than 100 nm relatively to the control experiment (no ligand) and the maximal response (here 6P4-RANTES), indeed correlates well with the relative magnitude of G protein signalling (Fig. 5a, red crosses). This conclusion differs from our recent observations on ligand-induced arrestin 2 clustering (Truan et al. 2013), where a connection between arrestin 2 clustering and CCR5 internalization had been established (Fig. 5b, blue circles). Arrestin 2 and arrestin 3 have been found to be interchangeable with respect to their function in many instances, in particular regarding receptor

desensitization and internalization (Pierce and Lefkowitz 2001). In the case of CCR5, Aramori et al. (1997) demonstrated that both arrestin 2 and arrestin 3 are sufficient (in conjunction with G protein-coupled receptor kinases) for the chemokine agonist MIP-1 $\beta$ /CCL4 to induce CCR5 internalization, with arrestin 3 being slightly more efficient than arrestin 2. Functional differences between the two homologues depending on some particular GPCR have, however, also been described (Pierce and Lefkowitz 2001). Arrestin 3 has, for example, been shown to induce  $\beta_2$ -adrenergic receptor internalization upon binding of the full agonist isoproterenol 100 times more efficiently than arrestin 2 (Kohout et al. 2001).

With CCR5 and the tested set of ligands, differences in the relative magnitude of arrestin 2 and arrestin 3 recruitment are actually minor but for one case: RANTES and PSC-RANTES, which induce strong arrestin 2 clustering, also lead to strong arrestin 3 clustering, and 5P12-RANTES does not cause mobilization of either of them; 5P14-RANTES, however, appears capable of mediating selectively clustering of arrestin 2, not of arrestin 3. One caveat to this observation is the background clustering detected in our assay (cells not exposed to any ligand), and one cannot totally exclude that 5P14-RANTES elicits an arrestin 3 response, which is too weak to be measured. This background level is, however, not significantly different from what was observed with arrestin 2 (Truan et al. 2013). 5P14-RANTES might, therefore, represent the first CCR5 ligand that is biased for one arrestin over another or G proteins, which would only hint again (Gaertner et al. 2008a; Truan et al. 2013) to the ability of this molecule to stabilize

a very special set of CCR5 conformations in comparison with other ligands. Biochemical experiments or other biophysical assays based on the bioluminescence resonance energy transfer (BRET) technology (Bertrand et al. 2002) might be able to provide a more definitive answer to this question in the future.

**Acknowledgments** We thank Jeffrey Benovic (Thomas Jefferson University) for the arrestin 3-GFP plasmid. This work was supported by the Swiss National Science Foundation through *Ambizione* fellowship PZ00P3\_131935 (A.F.) and project number 310030\_143789 (O.H.), as well as by Fondation Dormeur (O.H. and A.F.). M.H. acknowledges funding by the Bundesministerium für Bildung und Forschung (Grant Number 0315262) and the German Science Foundation (EXC 115).

## References

- Aramori I, Zhang J, Ferguson SSG, Bieniasz PD, Cullen BR, Caron MG (1997) Molecular mechanism of desensitization of the chemokine receptor CCR-5: receptor signaling and internalization are dissociable from its role as an HIV-1 co-receptor. *EMBO J* 16(15):4606–4616
- Banterle N, Khanh Huy B, Lemke EA, Beck M (2013) Fourier ring correlation as a resolution criterion for super-resolution microscopy. *J Struct Biol* 183(3):363–367
- Bertrand L, Parent S, Caron M, Legault M, Joly E, Angers S, Bouvier M, Brown M, Houle B, Menard L (2002) The BRET2/arrestin assay in stable recombinant cells: a platform to screen for compounds that interact with G protein-coupled receptors (GPCRs). *J Recept Signal Transduct Res* 22(1–4):533–541
- Betzig E, Patterson GH, Sougrat R, Lindwasser OW, Olenych S, Bonifacino JS, Davidson MW, Lippincott-Schwartz J, Hess HF (2006) Imaging intracellular fluorescent proteins at nanometer resolution. *Science* 313(5793):1642–1645
- Bockenhauer S, Fürstenberg A, Yao XJ, Kobilka BK, Moerner WE (2011) Conformational dynamics of single G protein-coupled receptors in solution. *J Phys Chem B* 115(45):13328–13338
- Cordes T, Strackharn M, Stahl SW, Summerer W, Steinhauer C, Forthmann C, Puchner EM, Vogelsang J, Gaub HE, Tinnefeld P (2010) Resolving single-molecule assembled patterns with super-resolution blink-microscopy. *Nano Lett* 10(2):645–651
- Endesfelder U, Finan K, Holden SJ, Cook PR, Kapanidis AN, Heilemann M (2013) Multi-scale spatial organization of RNA polymerase in *Escherichia coli*. *Biophys J* 105(1):172–181
- Escola J-M, Kuenzi G, Gaertner H, Foti M, Hartley O (2010) CC chemokine receptor 5 (CCR5) desensitization—cycling receptors accumulate in the trans-golgi network. *J Biol Chem* 285(53):41772–41780
- Fürstenberg A, Heilemann M (2013) Single-molecule localization microscopy—near-molecular spatial resolution in light microscopy with photoswitchable fluorophores. *Phys Chem Chem Phys* 15(36):14919–14930
- Gaertner H, Cerini F, Escola J-M, Kuenzi G, Melotti A, Offord R, Rossitto-Borlat I, Nedellec R, Salkowitz J, Gorochoy G, Mosier D, Hartley O (2008a) Highly potent, fully recombinant anti-HIV chemokines: reengineering a low-cost microbicide. *Proc Natl Acad Sci USA* 105(46):17706–17711
- Gaertner H, Lebeau O, Borlat I, Cerini F, Dufour B, Kuenzi G, Melotti A, Fish RJ, Offord R, Springael JY, Parmentier M, Hartley O (2008b) Highly potent HIV inhibition: engineering a key anti-HIV structure from PSC-RANTES into MIP-1 beta/CCL4. *Protein Eng Des Sel* 21(2):65–72
- Gesty-Palmer D, Luttrell LM (2011) Refining efficacy: exploiting functional selectivity for drug discovery. *Adv Pharmacol* 62:79–107
- Hartley O, Gaertner H, Wilken J, Thompson D, Fish R, Ramos A, Pastore C, Dufour B, Cerini F, Melotti A, Heveker N, Picard L, Alizon M, Mosier D, Kent S, Offord R (2004) Medicinal chemistry applied to a synthetic protein: development of highly potent HIV entry inhibitors. *Proc Natl Acad Sci USA* 101(47):16460–16465
- Heilemann M, van de Linde S, Mukherjee A, Sauer M (2009) Super-resolution imaging with small organic fluorophores. *Angew Chem Int Ed* 48(37):6903–6908
- Hell SW (2007) Far-field optical nanoscopy. *Science* 316(5828):1153–1158
- Hess ST, Girirajan TPK, Mason MD (2006) Ultra-high resolution imaging by fluorescence photoactivation localization microscopy. *Biophys J* 91(11):4258–4272
- Karim QA, Karim SSA, Frohlich JA, Grobler AC, Baxter C, Mansoor LE, Kharsany ABM, Sibeko S, Mlisana KP, Omar Z, Gengiah TN, Maarschalk S, Arulappan N, Mlotshwa M, Morris L, Taylor D, Grp CT (2010) Effectiveness and safety of tenofovir gel, an antiretroviral microbicide, for the prevention of HIV infection in women. *Science* 329(5996):1168–1174
- Kenakin T, Christopoulos A (2013) Signalling bias in new drug discovery: detection, quantification and therapeutic impact. *Nat Rev Drug Discov* 12(3):205–216
- Kenakin T, Watson C, Muniz-Medina V, Christopoulos A, Novick S (2012) A simple method for quantifying functional selectivity and agonist bias. *ACS Chem Neurosci* 3(3):193–203
- Kobilka BK, Deupi X (2007) Conformational complexity of G-protein-coupled receptors. *Trends Pharmacol Sci* 28(8):397–406
- Kohout TA, Lin FT, Perry SJ, Conner DA, Lefkowitz RJ (2001) Beta-arrestin 1 and 2 differentially regulate heptahelical receptor signaling and trafficking. *Proc Natl Acad Sci USA* 98(4):1601–1606
- Kuhmann SE, Hartley O (2008) Targeting chemokine receptors in HIV: A status report. *Annu Rev Pharmacol Toxicol* 48:425–461
- Laporte SA, Oakley RH, Holt JA, Barak LS, Caron MG (2000) The interaction of beta-arrestin with the AP-2 adaptor is required for the clustering of beta(2)-adrenergic receptor into clathrin-coated pits. *J Biol Chem* 275(30):23120–23126
- Lederman MM, Veazey RS, Offord R, Mosier DE, Dufour J, Mefford M, Piatak M Jr, Lifson JD, Salkowitz JR, Rodriguez B, Blauvelt A, Hartley O (2004) Prevention of vaginal SHIV transmission in rhesus macaques through inhibition of CCR5. *Science* 306(5695):485–487
- Lee SF, Vérolet Q, Fürstenberg A (2013) Improved super-resolution microscopy with oxazine fluorophores in heavy water. *Angew Chem Int Ed Engl* 52(34):8948–8951
- Lefkowitz RJ, Shenoy SK (2005) Transduction of receptor signals by beta-arrestins. *Science* 308(5721):512–517
- Luttrell LM, Ferguson SSG, Daaka Y, Miller WE, Maudsley S, Della Rocca GJ, Lin FT, Kawakatsu H, Owada K, Luttrell DK, Caron MG, Lefkowitz RJ (1999) Beta-arrestin-dependent formation of beta(2) adrenergic receptor Src protein kinase complexes. *Science* 283(5402):655–661
- Malkusch S, Endesfelder U, Mondry J, Gelleri M, Verveer PJ, Heilemann M (2012) Coordinate-based colocalization analysis of single-molecule localization microscopy data. *Histochem Cell Biol* 137(1):1–10
- Malkusch S, Muranyi W, Muller B, Krausslich HG, Heilemann M (2013) Single-molecule coordinate-based analysis of the morphology of HIV-1 assembly sites with near-molecular spatial resolution. *Histochem Cell Biol* 139(1):173–179
- Moerner WE (2012) Microscopy beyond the diffraction limit using actively controlled single molecules. *J Microsc* 246(3):213–220
- Moore CAC, Milano SK, Benovic JL (2007) Regulation of receptor trafficking by GRKs and arrestins. *Annu Rev Physiol* 69:451–482



- Mundell SJ, Matharu AL, Kelly E, Benovic JL (2000) Arrestin isoforms dictate differential kinetics of A(2B) adenosine receptor trafficking. *Biochemistry* 39(42):12828–12836
- Nieuwenhuizen RP, Lidke KA, Bates M, Puig DL, Grunwald D, Stallina S, Rieger B (2013) Measuring image resolution in optical nanoscopy. *Nat Methods* 10:557–562
- Owen DM, Williamson DJ, Boelen L, Magenau A, Rossy J, Gaus K (2013) Quantitative analysis of three-dimensional fluorescence localization microscopy data. *Biophys J* 105(2):L05–L07
- Pierce KL, Lefkowitz RJ (2001) Classical and new roles of beta-arrestins in the regulation of G-protein-coupled receptors. *Nat Rev Neurosci* 2(10):727–733
- Rask-Andersen M, Almen MS, Schioth HB (2011) Trends in the exploitation of novel drug targets. *Nat Rev Drug Discov* 10(8):579–590
- Ries J, Kaplan C, Platonova E, Eghlidi H, Ewers H (2012) A simple, versatile method for GFP-based super-resolution microscopy via nanobodies. *Nat Methods* 9(6):582–584
- Ripley BD (1977) Modelling spatial patterns. *J Roy Statist Soc B* 39:172–212
- Rosenbaum DM, Rasmussen SGF, Kobilka BK (2009) The structure and function of G-protein-coupled receptors. *Nature* 459(7245):356–363
- Rust MJ, Bates M, Zhuang XW (2006) Sub-diffraction-limit imaging by stochastic optical reconstruction microscopy (STORM). *Nat Methods* 3(10):793–795
- Santini F, Gaidarov I, Keen JH (2002) G protein-coupled receptor/arrestin3 modulation of the endocytic machinery. *J Cell Biol* 156(4):665–676
- Sengupta P, Jovanovic-Talisman T, Skoko D, Renz M, Veatch SL, Lippincott-Schwartz J (2011) Probing protein heterogeneity in the plasma membrane using PALM and pair correlation analysis. *Nat Methods* 8(11):969–975
- Smith CS, Joseph N, Rieger B, Lidke KA (2010) Fast, single-molecule localization that achieves theoretically minimum uncertainty. *Nat Methods* 7(5):373–375
- Specht CG, Izeddin I, Rodriguez PC, El Beheiry M, Rostaing P, Darzacq X, Dahan M, Triller A (2013) Quantitative nanoscopy of inhibitory synapses: counting gephyrin molecules and receptor binding sites. *Neuron* 79(2):308–321
- Truan Z, Tarancón Díez L, Bönsch C, Malkusch S, Endesfelder U, Munteanu M, Hartley O, Heilemann M, Fürstenberg A (2013) Quantitative morphological analysis of arrestin 2 clustering upon G protein-coupled receptor stimulation by super-resolution microscopy. *J Struct Biol* 184(2):329–334
- Wolter S, Schüttelpelz M, Tscherepanow M, Van de Linde S, Heilemann M, Sauer M (2010) Real-time computation of subdiffraction-resolution fluorescence images. *J Microsc* 237(1):12–22
- Zidar DA (2011) Endogenous ligand bias by chemokines: implications at the front lines of infection and leukocyte trafficking. *Endocr Metab Immune Disord Drug Targets* 11(2):120–131